INTERFACE

rsif.royalsocietypublishing.org

Research

Cite this article: Wenbo L, Wang J. 2017 Uncovering the underlying mechanism of cancer tumorigenesis and development under an immune microenvironment from global quantification of the landscape. *J. R. Soc. Interface* **14**: 20170105.
http://dx.doi.org/10.1098/rsif.2017.0105

Received: 12 February 2017
Accepted: 2 June 2017

Subject Category:
Life Sciences–Physics interface

Subject Areas:
biophysics, systems biology

Keywords:
potential landscape, cancer–immune network, tumorigenesis, cancer development

Author for correspondence:
Jin Wang
e-mail: jin.wang.1@stonybrook.edu

Electronic supplementary material is available online at https://dx.doi.org/10.6084/m9.figshare.c.3801442.

THE ROYAL SOCIETY PUBLISHING

Uncovering the underlying mechanism of cancer tumorigenesis and development under an immune microenvironment from global quantification of the landscape

Li Wenbo[1] and Jin Wang[1,2,3]

[1]State Key Laboratory of Electroanalytical Chemistry, Changchun Institute of Applied Chemistry, Chinese Academy of Sciences, Changchun, Jilin, People's Republic of China
[2]Department of Chemistry, and [3]Department of Physics, State University of New York at Stony Brook, Stony Brook, NY, USA

LW, 0000-0002-8642-9857

The study of the cancer–immune system is important for understanding tumorigenesis and the development of cancer and immunotherapy. In this work, we build a comprehensive cancer–immune model including both cells and cytokines to uncover the underlying mechanism of cancer immunity based on landscape topography. We quantify three steady-state attractors, normal state, low cancer state and high cancer state, for the innate immunity and adaptive immunity of cancer. We also illustrate the cardinal inhibiting cancer immunity interactions and promoting cancer immunity interactions through global sensitivity analysis. We simulate tumorigenesis and the development of cancer and classify these into six stages. The characteristics of the six stages can be classified further into three groups. These correspond to the escape, elimination and equilibrium phases in immunoediting, respectively. Under specific cell–cell interactions strength oscillations emerge. We found that tumorigenesis and cancer recovery processes may need to go through cancer–immune oscillation, which consumes more energy. Based on the cancer–immune landscape, we predict three types of cells and two types of cytokines for cancer immunotherapy as well as combination immunotherapy. This landscape framework provides a quantitative way to understand the underlying mechanisms of the interplay between cancer and the immune system for cancer tumorigenesis and development.

1. Introduction

The immune system is a complex one which protects against disease, for example, by eliminating tumour cells. When tumour cell antigens are detected by the immune system this leads to the innate immune response and the adaptive immune response, both of which are involved in many types of immune cells and cytokines [1]. However, during tumorigenesis and progression, cancer can lead to dysfunction of the immune system. The immune system can then become an accomplice through chronic inflammation [2]. This leads to two hallmarks of cancer immunity, avoiding immune destruction and tumour-promoting inflammation [3]. The functions of the immune system during cancer development are complicated, thus studying the underlying mechanisms between cancer and the immune system is important for understanding cancer and cancer therapy. Recent studies on immune vaccines suggest that it is crucial to find an effective immune therapy [4].

Mathematical models are useful and effective for describing intricate systems such as the tumour immune microenvironment. Many immunity models have been studied. In [5], a few spatially homogeneous mechanistic mathematical models were reviewed, and a summary of different models from single-variable

to multi-variable models is given. The relationship between the immune response and cancer aggressiveness was studied through a specific model. Tumour and immune cells were studied with an exosome exchange model to assess the effectiveness of different therapeutic protocols [6]. Besides cancer mechanistic studies, mathematic models are also used to study immune cell vaccines [7]. Although many immune models have been built using ordinary differential equations (ODEs), a comprehensive immune model including both immune cells and cytokines for cancer from a biological network perspective has not yet been established.

Quantitative analysis of a circuit or complex network is important for characterizing biological processes and their underlying mechanisms. These can be quantitatively studied physically and globally through the landscape and flux theory of non-equilibrium dynamic systems [8–10]. The theory has been applied to different fields, including gene regulation networks [9,11–14], neural networks [15,16], metabolism pathways [17], signalling networks [18], evolution [19] and ecology [20]. However, it is still challenging to reveal the underlying mechanism between cancer and the immune system.

In this work, we build comprehensive cancer–immune networks by collecting data from the experimental literature [21–36]. The network includes cancer cells, 12 types of immune cells and 13 types of cytokines. The network involves cell–cell interactions, cytokine–cell interactions and cell–cytokine production. We have analysed the immune network quantitatively. Three steady-state basins of attractor, normal state, low cancer state and high cancer state emerge based on the landscape topography. Along with cancer development and evolution, the landscape presents different characteristics corresponding to the different phases in immunoediting [37]. We also uncover the emergence and origin of cancer–immune oscillations. Important immunotherapy targets are predicted, including three types of immune cells and two types of cytokines.

2. Results

2.1. Cancer–immune system network modelling

Different cancer types are influenced by immune cells and cytokines differently. For example, $CD8^+$ T cells ($CD8^+$) attack MHC-I-positive tumour cells, while natural killer (NK) cells attack tumour cells with MCH-I loss or downregulation [38]. Here, in our model, we consider tumour cells to be heterogeneous. The network includes cell–cell interactions, cytokine–cell interactions and cell–cytokine production. All these relationships are from previous experimental studies [21–36]. The cancer–immune network includes cancer cells, T helper cells (Th1, Th2 and Th17), macrophage cells (M1 and M2), tumour-associated neutrophil cells (TAN), myeloid-derived suppressor cells (MDSCs), $CD8^+$, regulatory T cells (Treg), dendritic cells (mature dendritic cells and immature dendritic cells) and NK cells as well as 13 related cytokines, interleukin (IL)-2, IL-4, IL-6, IL-8, IL-10, IL-12, IL-13, IL-17, IL-21, IL-23, interferon (IFN)-γ, transforming growth factor (TGF)-β and tumour necrosis factor (TNF)-α with a total of 26 nodes. The interactions among the nodes are listed in the electronic supplementary material, table S1.

We chose representative immune cells and their associated cytokines closely related to cancer cells for the immune response from the existing literature. We also selected the regulations among these cancer cells, immune cells and cytokines from the literature search.

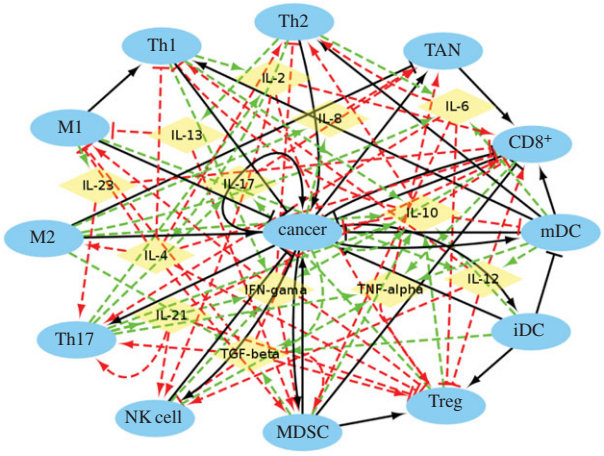

Figure 1. The cancer–immune system. The network includes 26 nodes and 107 interaction links. Cerulean ellipses represent cells and yellow diamonds represent cytokines. Black solid arrows and bars represent cell–cell activation and inhibition, respectively. Red dashed arrows and bars represent cytokine–cell activation and inhibition, respectively. Green dashed arrows represent cell–cytokine production.

Dendritic cells (mDCs) are antigen-presenting cells of the immune system. They trigger the adaptive responses when detecting antigens from cancer cells. Immature dendritic cells (iDCs) have been considered suppressive and tolerogenic to cancer immunity [32]. NK cells and $CD8^+$ are the main effective killer cells for the innate immune response and the adaptive immune response, respectively. T helper cells are central to the development of an immune response by activating antigen-specific effector cells and recruiting cells of the innate immune system. Th1 cells activate antigen-presenting cells (APCs) and induce the production of the type of antibodies that can enhance the chances of cancer cells turning into APCs. However, the Th2 response triggered by cancer promotes the growth of cancer cells [34]. Th17 cells play a potent proinflammatory role in cancer microenvironments [25]. M1 plays a classic role in the Th1 response and in mediating resistance against cancer cells. M2 takes part in the inflammatory process [23]. In addition, TAN plays an important role in tumour growth and progression [23].

It is evident that immune responses in cancer are negatively regulated by immunosuppressive cells (Treg) and MDSCs [28]. Cytokines are produced by the cells and regulate other cells through activation or repression. Cytokines can thus mediate the cell–cell interactions. The different cytokines are chosen according to different cell types for the network building. The whole network is shown in figure 1.

For the major cell–cell interactions, Th1 inhibits cancer cells by activating the APCs, while Th2 activates cancer cells by promoting their proliferation. M1 activates Th1 and inhibits cancer cells. M2 activates cancer cells through an inflammatory process [23]. $CD8^+$, Th1 and Th2 are activated by mDCs. Accumulation of iDCs inhibits mDC proliferation and activates Treg through stimulating its proliferation [26]. TAN activates $CD8^+$ by enhancing proliferation [33]. The cancer cells and MDSCs form a positive feedback loop through PGE2 and COX-2. MDSCs activate Treg by inducing its expansion through the ARG1 pathway. MDSCs inhibit the $CD8^+$ response [28]. NK cells and $CD8^+$

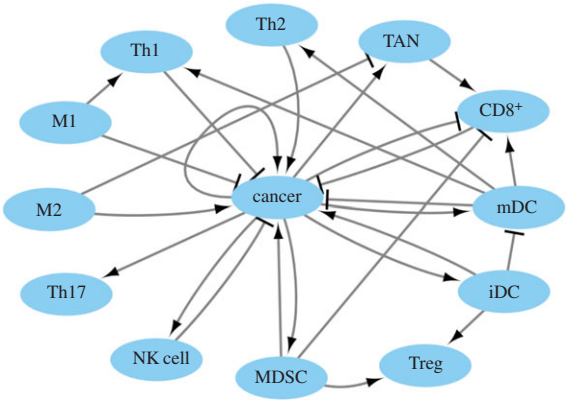

Figure 2. The cancer–immune system for cell–cell interactions. Black arrows represent cell–cell activation. Black bars represent cell–cell inhibition.

inhibit cancer cells as effective killers. The cancer->cancer interaction does not just refer to the cancer growth by itself. It can be activated by the self-production of cytokines, such as IL-1 [34], which is not included in the cancer–immune network in order to avoid redundancy.

For the major cytokine–cell interactions, Th1 is mainly activated by IL-2. Th2 is mainly activated by IL-4. IL-12 activates NK cells and $CD8^+$. NK cells and MDSCs are mainly activated by IL-17 [21,25]. Th17 is mainly activated by IL-21 and IL-23 through triggering expansion [25]. M1 is mainly activated by IFN-γ [34]. For the main cytokine production, IL-17 is mainly produced by Th17 [21]. TGF-β leads to cancer proliferation [28]. Owing to the complexity of the network for viewing the whole map clearly, we also display only the cell–cell interactions in figure 2.

The driving forces of the dynamics for the cell or cytokine concentrations are determined as

$$F(X_i) = A_i \prod_{j=1}^{N_i} H_{ji} - D_i X_i \prod_{j=1}^{N_i'} H_{ji}, \tag{2.1}$$

$$F(X_i) = A_i \sum_{j=1}^{N_i} \frac{X_j^n}{S_{ji}^n + X_j^n} - D_i X_i \tag{2.2}$$

and

$$H_{ji} = \frac{S_{ji}^n}{S_{ji}^n + X_j^n} + \gamma_{ji} \frac{X_j^n}{S_{ji}^n + X_j^n} \tag{2.3}$$

$$= (\gamma_{ji} - 1) \frac{X_j^n}{S_{ji}^n + X_j^n} + 1 \tag{2.4}$$

$$= (1 - \gamma_{ji}) \frac{S_{ji}^n}{S_{ji}^n + X_j^n} + \gamma_{ji}, \tag{2.5}$$

where F represents the driving force of the variable X, the effector cell concentration or the cytokine concentration. The characteristics of cell–cell and cytokine–cell interactions are different from those of cell–cytokine production. Equation (2.1) is used for cell–cell and cytokine–cell interactions, while equation (2.2) is used for cell–cytokine production. In equation (2.1), X represents the effector cell concentration, and A represents the basic production rate of the cell concentration. In equation (2.2), X represents the cytokine concentration, and A represents the maximum production rate of the cytokine concentration in the immune microenvironment. D represents the degradation rate of the cells or cytokine concentration and S represents the threshold with half concentration production. The parameter n is the Hill coefficient for describing the cooperativity of the interactions. The positive parameter γ_{ji} represents the activation of X_i from X_j if $\gamma > 1$ and inhibition if $\gamma < 1$. The Hill function was used for presenting cell–cell interactions and cytokine–cell interactions in [39,40]. For cell–cell or cytokine–cell interactions, H_{ji} is the summation of the two Hill functions, the inhibition term and the activation term. When $\gamma > 1$, equation (2.3) can be converted into equation (2.4), and the activation term (only the second term) is effective. Conversely, when $\gamma < 1$, equation (2.3) can be converted into equation (2.5), and only the inhibition term is effective. Owing to the saturation effects of the immune response [40], the Hill function H_{ji} is used to approximately represent the cell production rate change upon interacting with other cells or cytokines in our model. This is because the immune cells communicate through surface receptors and the regulation is saturated due to the limit in the quantity of the surface receptors. The product of H_{ji} represents the combined effect of both the cell–cell and cytokine–cell interactions. For the cell–cytokine production, the whole production is described by the summation of the Hill functions. Michaelis–Menten form is used to describe cell–cytokine interactions with limited production of cytokines [40]. We consider that the maximum production rate in the cancer microenvironment is limited, because the cytokines generated from the cancer microenvironment diffuse to a healthy part of the tissue. Every Michaelis–Menten term in equation (2.2) represents the contribution of the production rate for every related cell. Each type of cytokine produces the total maximum production rate A. Specifically, the term H_{ji} used for multiplying $D_i X_i$ in equation (2.1) is only for interactions on cancer cells from NK cells and $CD8^+$. Because the NK cells and $CD8^+$ are killer cells corresponding to the innate immune system and the adaptive immune system, respectively, the inhibiting mechanism promotes the decay of cancer cells.

The parameters for this cancer–immune model are chosen carefully to produce results that are biologically relevant and reasonable. For example, the decay rate is set according to the death rates for most types of cells. We also take into consideration the differences in activation or inhibition strengths between cell types and in order to reasonably describe the interactions in the cancer–immune system according to the previous experimental studies. For example, both IL-4 and IL-6 promote Th2, and it is mainly triggered by IL-4 [36], thus we set the IL-4->Th2 activation regulation strength much higher than the IL-6->Th2 activation regulation strength. For other interactions lacking such information we just set the regulations at the same level. The interaction strengths and corresponding references are listed in the electronic supplementary material, table S2.

2.2. Landscape of cancer innate and adaptive immunity

The landscape of the cancer–immune system can be obtained through the self-consistent mean field approximation of the corresponding probabilistic evolution equation. The landscape $U = -\ln(P_{ss})$, where U is defined as the landscape and is directly related to P_{ss}, which represents the steady-state probability distribution of the concentration variables.

The ODEs of the cancer–immune system includes 26 variables. It is difficult to visualize the landscape in 26 dimensions. We chose two dimensions to display by integrating

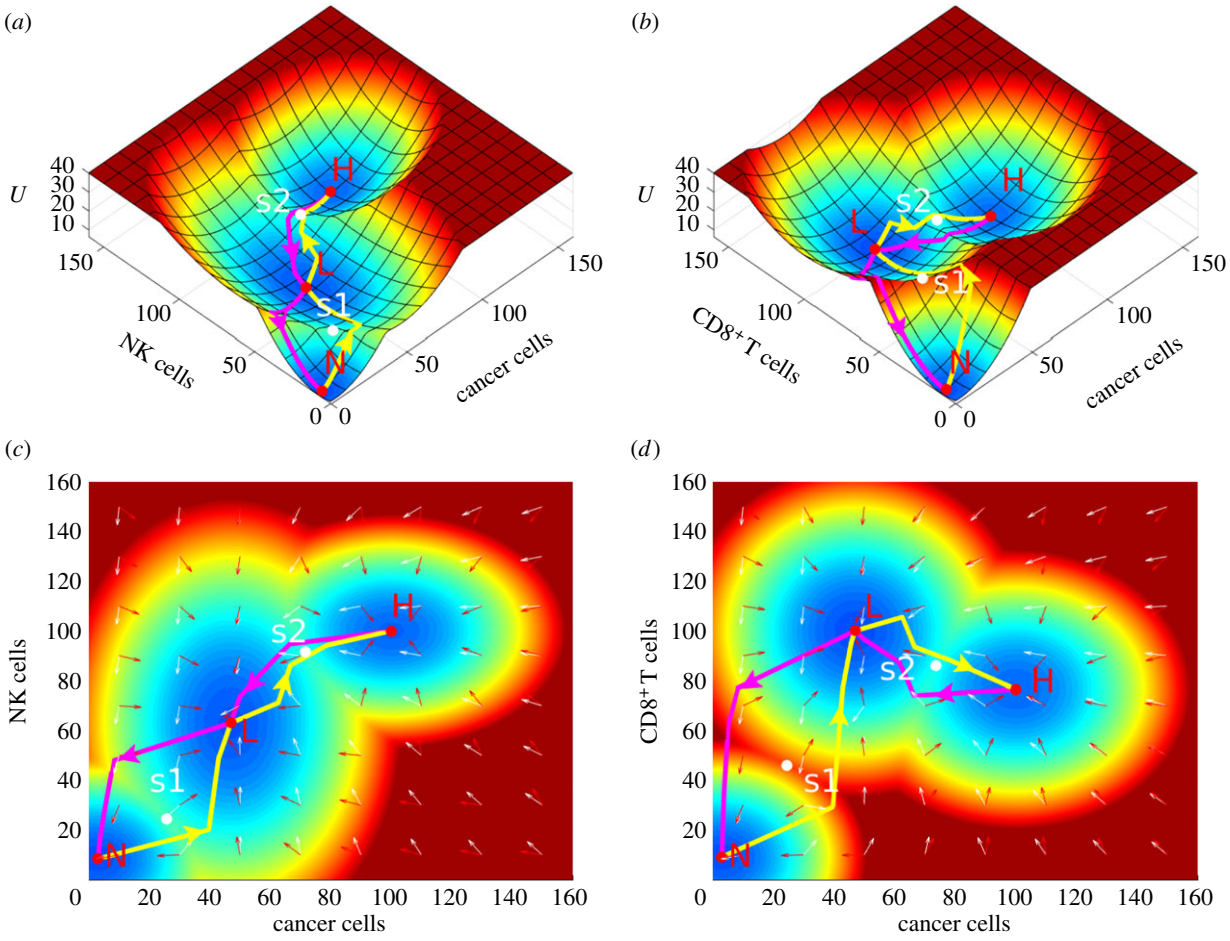

Figure 3. The landscape of the cancer innate immune and adaptive immune system. The cancer innate immune system is depicted by cancer cells and NK cells in (*a*,*c*). The cancer adaptive immune system is depicted by cancer cells and $CD8^+$ in (*b*,*d*). N, normal state; L, low cancer state; H, high cancer state; s1, saddle between the normal state and the low cancer state; s2, saddle between the normal state and the high cancer state. The yellow arrows represent the paths from N to L and from L to H, and the magenta arrows represent the paths from H to L and from L to N. The white arrows represent the directions of probability flux, and the red arrows represent the directions of the negative gradient of potential energy. (*c*,*d*) Same landscape in two dimensions for (*a*,*b*), respectively.

over other dimensions. We chose effective killer cells and the cancer cell as the two-dimensional variables. The immune system includes the innate immune system and the adaptive immune system. The innate immune system gives an immediate and non-specific response to the pathogens, while the adaptive system resorts to APCs, such as dendritic cells for responding, and is highly specific to a particular pathogen. The main effective killer cells of the innate immune system are NK cells and the main effective killer cells of the adaptive immune system are $CD8^+$. In order to show the different characteristics between the innate immune system and the adaptive immune system, cancer cells with NK cells and with $CD8^+$ are separately chosen for landscape display. Three steady-state attractors, normal state (N), low cancer state (L) and high cancer state (H), emerge as shown in figure 3. The red region represents high potential, while the blue region represents low potential. Between the two steady-state attractors, there is a saddle which is coloured white in figure 3. We define the saddle between the normal state and the low cancer state as s1 and the saddle between the low cancer state and the high cancer state as s2.

The landscape of the innate immune variable is displayed in figure 3*a*,*c*, whereas the adaptive immune variable is shown in figure 3*b*,*d*. The landscape characteristics of the innate immune and the landscape characteristics of the adaptive immune variables are not the same. In the normal state (N), cancer cells, NK cells and $CD8^+$ are all at very small concentrations (near zero). For the innate immune response, the NK cells are at low (high) level with respect to the low (high) cancer state. On the other hand, for the adaptive immune response, the $CD8^+$ are at high (low) level with respect to the low (high) cancer state. The result on the adaptive response is also observed in other immune models [41]. This suggests that, at the high cancer state, the adaptive immune response is inhibited by cancer cells.

To study the transition processes among steady-state attractors, we calculated the dominant paths among different attractors by minimizing the transition actions. The dominant paths are shown on the landscape (figure 3*b*,*d*). The yellow arrows (from the N (normal) state to the L (low cancer) state and from the L state to the H (high cancer) state) represent tumorigenesis and the transition to a high cancer state, while the magenta arrows (from the H state to the L state and from the L state to the N state) represent cancer recovery. We also show the steady-state probability flux of the cancer–immune system on the landscape in figure 3*c*,*d*. The white and red arrows, respectively, represent the direction of probability flux and the negative gradient of the potential energy. The dynamics of the cancer–immune system is determined by both the gradient of the potential and the probability flux. The force from the steady-state probability flux

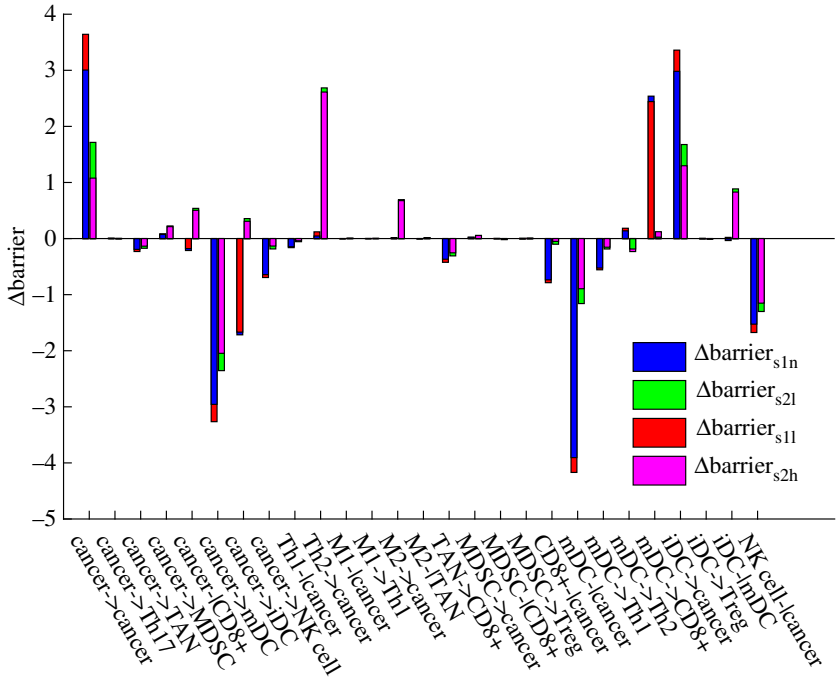

Figure 4. Global sensitivity analysis for the 27 cell–cell interactions. The *x*-axis represents the 27 cell–cell interactions. The *y*-axis represents the barrier changes. Each parameter is increased by 10% individually. $\Delta barrier_{s1n}$, the change of barrier between s1 and the normal steady state. $\Delta barrier_{s1l}$, the change of barrier between s1 and the low cancer state. $\Delta Barrier_{s2l}$, the change of barrier between s2 and the low cancer steady state. $\Delta Barrier_{s2h}$, the change of barrier between s2 and the high cancer steady state.

leads the dominant paths of the system to deviate from the conventionally expected potential gradient paths. As we can see the two dominant paths are different from each other: cancer tumorigenesis/transition to the high cancer state and cancer recovery are irreversible.

2.3. Global sensitivity analysis of the cancer immunity model

We define the potential between the saddle and the steady-state attractor as the barrier height. This represents the ability to switch from one steady-state attractor to another. According to figure 4, we can quantify the barrier between s1 and the normal steady state ($barrier_{s1n}$), the barrier between s1 and the low cancer steady state ($barrier_{s1l}$), the barrier between s2 and the low cancer steady state ($barrier_{s2l}$) and the barrier between s2 and the high cancer steady state ($barrier_{s2h}$). Each of the 27 cell–cell interaction parameters is increased by 10% for perturbing the network, leading to changes in the respective barrier. As shown in figure 4, every group has four barrier changes for each parameter change. We considered that the regulation parameters changes for promoting the low cancer state and inhibiting the normal state if the barrier changes of the low cancer state are larger than those of the normal state, because the low cancer state becomes more stable or less unstable compared with the normal state. In the same sense, the regulation parameter changes are for promoting the high cancer state and inhibiting the low cancer state if the barrier changes of the high cancer state are larger than those of the low cancer state.

Interestingly, all of these regulation parameters change for either promoting the low cancer steady state, or promoting the normal state and high cancer state but not both. The cell–cell interactions promoting the low cancer state are cancer->cancer, cancer->MDSC, cancer-|$CD8^+$, cancer->iDC, Th2->cancer, M2->cancer, M2-|TAN, MDSC->cancer, mDC->Th2, iDC->cancer, iDC->Treg and iDC-|mDC, most of which that inhibit cancer immunity were reported in [29,42–45]. The cell–cell interactions inhibiting the low cancer state, cancer->Th17, cancer->TAN, cancer->mDC, cancer->NK cell, Th1-|cancer, M1-|cancer, M1->Th1, TAN->$CD8^+$, MDSC-|$CD8^+$, MDSC->Treg, $CD8^+$-|cancer, mDC-|cancer, mDC->Th1, mDC->$CD8^+$ and NK cell-|cancer, were reported to show a trend of promoting cancer immunity [46–49]. This indicates that the low cancer state switches to the normal state or high cancer state under promoting cancer immunity. It perhaps implies that the underlying immune pressure is the force driving the low cancer state to the high cancer state. This means cancer cells have to die or evolve to the high cancer state in the cancer–immune system.

The low cancer steady state is thus used to characterize cancer immunity. From the global sensitivity analysis, we explore the barrier changes of the low cancer state and the normal state in figure 4. A greater difference in barrier change values means more influence by the cell–cell interactions with respect to the parameter changes. The cardinal inhibiting cancer immunity interactions are cancer->cancer and iDC->cancer, while the cardinal promoting cancer immunity interactions are cancer->mDC, mDC-|cancer, NK cell-|cancer and mDC->$CD8^+$.

2.4. Quantification of normal and cancer state kinetic switching

For these cardinal interactions, we chose cancer->cancer for further analysis as an example, because cancer cells are heterogeneous and cancer->cancer strength varies largely. The decay rate of cancer (D_{cancer}) is also varied. The barrier can be used to measure the ability to switch from one attractor to another. The mean first passage time (MFPT) is defined as the average transition time from one attractor to another. It is also used to measure the ability to switch. For example, if the MFPT from the normal state to the low cancer state (τ_{nl}) is longer than the

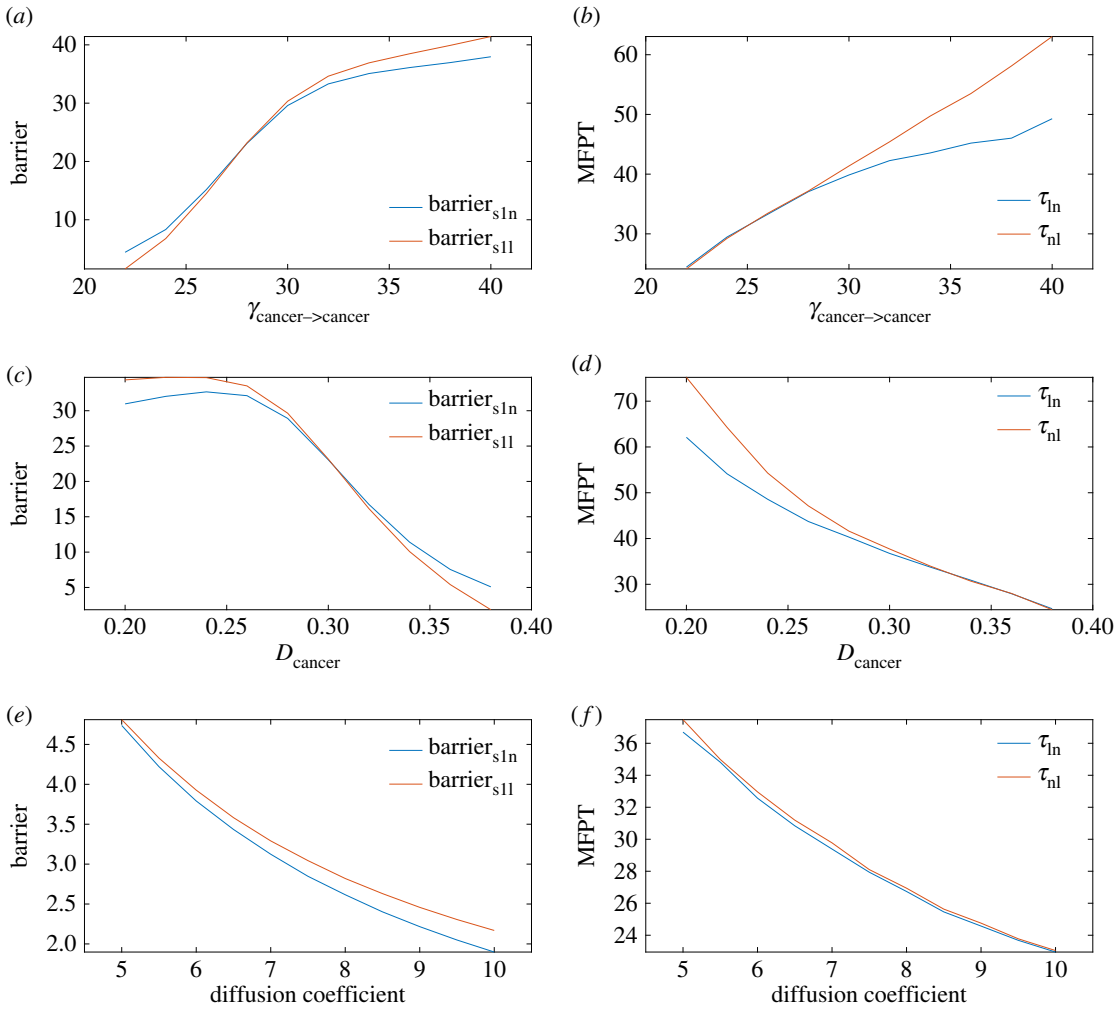

Figure 5. (*a–f*) The barrier and MFPT results when $\gamma_{\text{cancer->cancer}}$, D_{cancer} as well as the diffusion coefficient change; $\text{Barrier}_{\text{s1n}}$, the barrier between s1 and the normal state. $\text{Barrier}_{\text{s1l}}$, the barrier between s1 and the low cancer state. τ_{ln}, the mean first passage time from the low cancer state to the normal state. τ_{nl}, the mean first passage time from the normal state to the low cancer state.

adverse transition (τ_{ln}), the system prefers to stay in the normal state, which means there is less probability of encountering cancer. The barrier and MFPT calculations along with the $\gamma_{\text{cancer-> cancer}}$ (cancer–cancer cell interations) or D_{cancer} changes are shown in figure 5*a–d*. This figure shows that when $\gamma_{\text{cancer-> cancer}}$ is increased or D_{cancer} is decreased, $\text{barrier}_{\text{s1n}}$, $\text{barrier}_{\text{n1s}}$, τ_{ln} and τ_{nl} all increase. This suggests that the normal state and low cancer state both become more stable. It is interesting that the normal state becomes more stable when $\gamma_{\text{cancer-> cancer}}$ is increased or D_{cancer} is decreased. This may imply that cancer cells without immunity change will not lead to transitions between the normal state and the low cancer state. Figure 5*e,f* shows the landscape results when fluctuations characterized by the diffusion coefficient (noise level) are changed. This shows that, when the diffusion coefficient is increased, $\text{barrier}_{\text{s1n}}$, $\text{barrier}_{\text{n1s}}$, τ_{ln} and τ_{nl} all decrease. The normal state and low cancer state both become less stable. This suggests that, as the noise goes up, the transitions between the normal state and the low cancer state become easier.

2.5. Dynamic landscape of immunity along cancer development under an immune microenvironment

Immunity of cancer in the immune microenvironment evolves along with tumorigenesis and progression. Not only the concentration of cancer cells, but also the tumour-associated immune cells such as MDSC are increased during cancer development. This is controlled by the regulation interactions between different cells or cytokines and cells. In order to display the dynamic landscape changes and simulate cancer development, we increase the inhibiting cancer immunity and decrease the strength of the cell–cell interactions promoting cancer immunity at the same time. We simulate starting with strong cancer immunity, and all cell–cell interaction parameters inhibiting cancer immunity are multiplied by $\alpha(\alpha \geq 1)$ and all cell–cell interaction parameters promoting cancer immunity are divided by $\alpha(\alpha \geq 1)$ to represent the cancer development level.

The whole cancer development dynamic landscape is shown in figure 6. The top four and bottom two landscapes are shown in different ranges or scales to display different details. The cancer development direction is from top to bottom as α increases. When the cancer is at strong immunity ($\alpha = 1$), it is monostable and the cancer cells, NK cells and $CD8^+$ are at a low level. Only the normal state is distinct. Along with cancer development, the low cancer state emerges and the high cancer state emerges at $\alpha = 1.2$ and $\alpha = 1.3$, respectively. Although the high cancer state at $\alpha = 1.3$ emerges, the NK cells and $CD8^+$ levels are also increased compared with the low cancer state. For further cancer development, the high cancer state moves to a high-cancer–low-immunity state for $CD8^+$ ($\alpha = 1.4$), and the

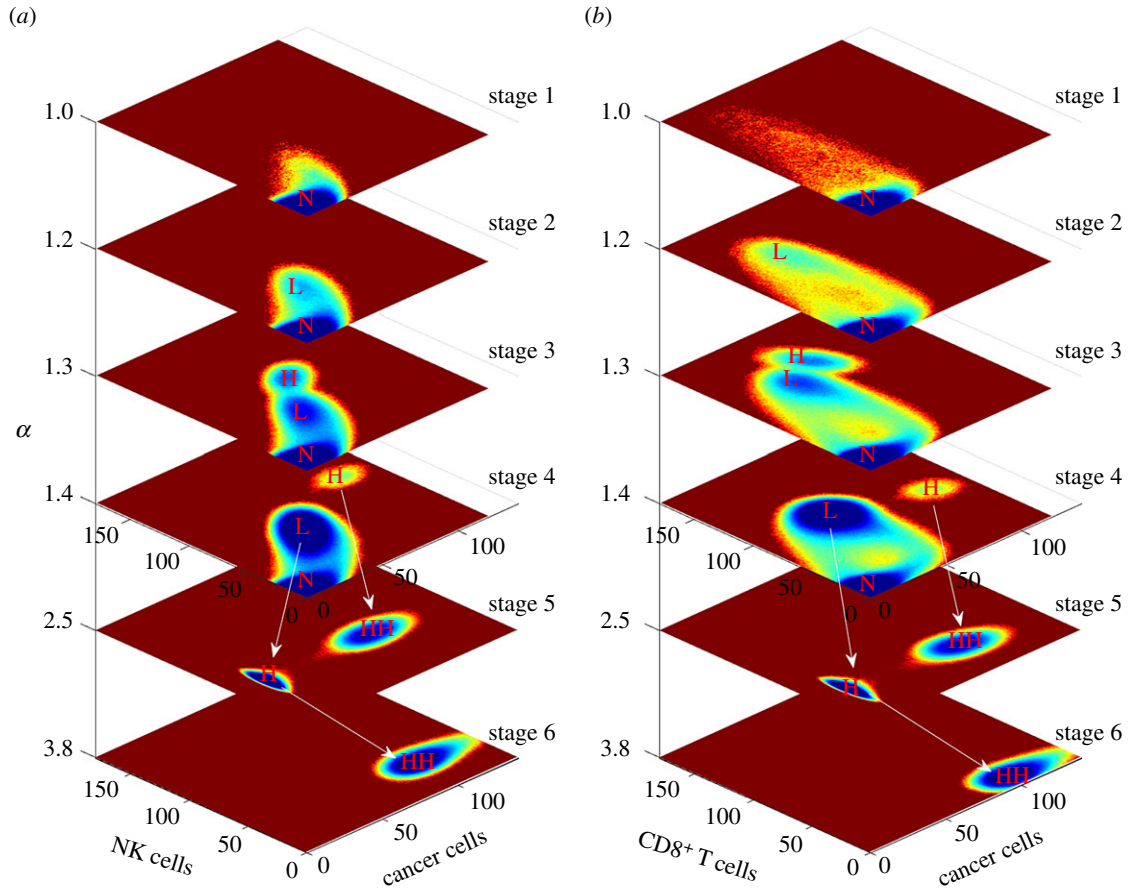

Figure 6. Dynamic landscape of cancer tumorigenesis and development. The horizontal coordinates represent cancer development along with increasing α from top to bottom. The top four stages and the bottom two stages are shown in different ranges of cancer cell concentration level. The cancer cell concentration in the bottom two stages ranges from 0 to 1400. The cancer cell concentration in the top four stages ranges from 0 to 140. The white arrows indicate the state moves between two stages: (*a*) dynamic landscape for cancer cells and NK cells and (*b*) dynamic landscape for cancer cells and $CD8^+$.

three states (normal, low cancer and high cancer) coexist, which corresponds to the result in [41]. Then, the normal state starts to disappear and the low cancer state moves to a high cancer state, while the high cancer state moves to a larger concentration level, which is defined as the high–high cancer state (HH) when $\alpha = 2.5$ with a low immunity level. Finally and interestingly, the steady-state attractor at HH disappears and the high cancer state continues to increase to the HH instead, as shown in figure 6, when $\alpha = 3.8$. The concentration level of HH continues growing when α is increased with a low immunity level.

Cancer development is a complex process along with DNA mutation and microenvironment changes. It is characterized by immunoediting [37], consisting of three phases: elimination, equilibrium and escape. In our model, it has six stages along with cancer tumorigenesis and process. At the stage of $\alpha = 1$, only the normal state emerges and it can be controlled by the immune system. The cancer concentration is impossible to reach at a higher level and the newborn cancer cells are killed immediately. This corresponds to the elimination phase. At the stage of $\alpha = 2.5$ and $\alpha = 3.8$ only high cancer or HH emerges and it will never switch back to the normal state. The cancer cell is out of control through escaping from immune cell detection and inhibition of immune cell activation. The cancer concentration level continues to increase rapidly along with cancer development. The two stages correspond to the escape phase. Equilibrium is the longest of the three processes in cancer immunoediting [37] and it involves the normal state and at least the low cancer state. The stages at $\alpha = 1.2$, $\alpha = 1.3$ and $\alpha = 1.4$ correspond to the equilibrium phase. During this phase, it is possible to switch between the normal state and other steady states owing to biological fluctuation. When it switches back to the normal state, most cancer cells are destroyed. The surviving cancer cells reproduce and evolve to a population with increased resistance to the immune system, leading to gradual cancer development. The final stage of the escape phase emerges when $\alpha = 1.4$, because the immune system starts to lose control of the cancer cells, as shown in figure 6.

It is interesting that tumorigenesis can start with a low cancer state and finally settles at HH even without direct transitions across barriers among steady-state attractors along cancer development. It seems that the low cancer state is the source while the high cancer state is the derivative along cancer development. The barriers between saddles and steady states under a tristable system along with cancer development are shown in figure 7. Barrier_{s1l} increases faster than barrier_{s1n}, while barrier_{s2l} increases faster than barrier_{s2h}. This suggests that the low cancer steady state becomes more stable along cancer development. Above all, it implies that the high cancer state is the product of evolution under immune pressure at the specific stages of development.

2.6. Cancer oscillation landscape

It is interesting that oscillation emerges when we explore the regulatory interactions cancer->cancer, cancer->mDC,

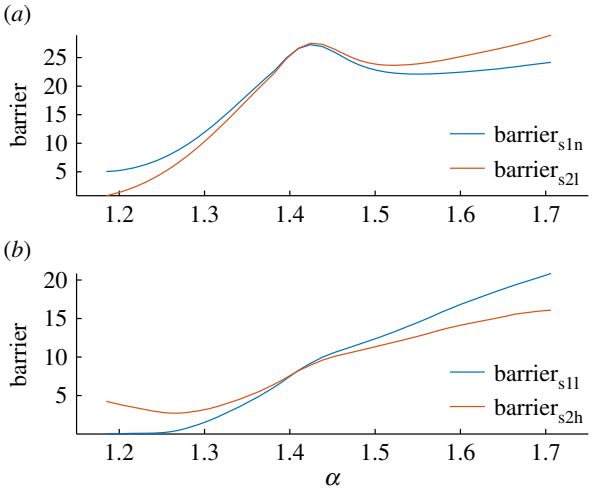

Figure 7. Barrier for a tristable cancer–immune system along with increasing α. $\Delta Barrier_{s1n}$, the change of barrier between s1 and the normal state. $\Delta Barrier_{s1l}$, the change of barrier between s1 and the low cancer state. $\Delta Barrier_{s2l}$, the change of barrier between s2 and the low cancer steady state. $\Delta Barrier_{s2h}$, the change of barrier between s2 and the high cancer steady state.

mDC->$CD8^+$ and $CD8^+$->cancer under specific conditions. The landscape is obtained using the Langevin method and one steady state with the limit cycle is obtained. When we increase the regulations of cancer->cancer or decrease the other three interactions starting with the monostable state, a shallow limit cycle emerges and, finally, switches to the low cancer state along with the regulation changes.

The oscillation has been observed in some related tumour and immune system studies [50,51]. The landscape under cancer->mDC regulation changes is shown in figure 8 as an example. In figure 8*b*, a shallow limit cycle emerges and circulates anticlockwise. The limit cycle seems to be a triangle. When the $CD8^+$ and cancer cells are at a relatively low level, the cancer concentration increases with a slight increase of $CD8^+$. When the cancer cells reach a relatively high level, $CD8^+$ start to increase rapidly, which leads to the cancer cells decreasing. When it reaches a state with a relatively high $CD8^+$ level and a relatively low cancer level, the $CD8^+$ level decreases rapidly. It then returns to the state with a relatively low $CD8^+$ and low cancer cell level. The limit cycle shrinks along the decrease of regulation in figure 8*c* and the potential landscape of the limit cycle near the low cancer state becomes deeper. Finally, it switches to the low cancer state in figure 8*d*. This suggests that the limit cycle can be a precursor of the low cancer state under some conditions.

It is interesting that the four interactions leading to the limit cycle become a module consisting of three nodes, cancer, mDCs and $CD8^+$, which is shown in the electronic supplementary material, figure S1. mDCs bridge innate immunity with adaptive immunity [52], while $CD8^+$ are the main effective killers for adaptive immunity. From the electronic supplementary material, figure S1, the cancer cell concentration is increased through self-activation and inhibited through the adaptive response. If we consider there is an indirect activation between cancer and $CD8^+$ by ignoring the mDCs it is quite similar to the classical predator–prey dynamics of an activation–repression loop, which leads to oscillation under specific regulations [53]. This suggests that promoting the cancer adaptive response module may lead to immunity oscillation.

In addition, we calculated the entropy production rate (EPR) for the phase transition from bistability to oscillation to monostability by increasing the regulation of cancer-> mDC (figure 8*e*). The EPR represents the total entropy variations. Decreasing the EPR means less energy for maintenance. We can see that the EPR is high when oscillation emerges. When the system switches to bistability or monostability, the EPR sharply decreases. This implies that the oscillation phase requires much more energy to maintain. We also calculated the flux integral and coherence of the system when the oscillation emerges (figure 8*f*). The flux integral correlates with coherence roughly. This indicates that the higher flux leads to high oscillation coherence. The flux integral and coherence decrease sharply when the system starts to switch to bistability or monostability. This indicates that a larger flux leads to a stronger driving force in the oscillation and more energy dissipation. Therefore, more energy has to be pumped into the system for switching between bistability and monostability. It also implies that cancer tumorigenesis and recovery processes consume more energy.

2.7. Cell and cytokine therapy target

Cancer immunotherapy uses the immune system to treat cancer. Recently, researchers have paid more attention to immunotherapy, and the recent achievements of several key immunotherapy milestones have dramatically changed the field of cancer treatment [54]. It is important to predict the effective immunotherapy target.

Here, we predict the immunotherapy target based on landscape theory. For each variable x_i, $F(x_i)$ is changed to $F'(x_i) = F(x_i) + c_i$. The term c_i represents the corresponding variable rate change by immune cell or cytokine injections. The potential energies of the three steady-state attractors are calculated for equivalent c_i. We define the changes of the relative potential energy from the normal state to the low cancer state as the degree of therapy effect. The normal state becomes more stable or less unstable compared with the low cancer state, if the changes in the relative potential energy are positive. The therapy takes the adverse effect, if the relative potential energy becomes negative.

The immune cells and the degree of cytokine therapy are shown in figure 9*a*,*b*. We predict three important therapy targets of immune cells: mDCs, NK cells and $CD8^+$. Although the tumour-associated cells also show a positive therapeutic effect, the injection of TAN cells makes the low cancer steady state more stable, as shown in the electronic supplementary material, figure S2, and it is not considered as a therapy target. It is reported that mDC vaccination reduces the size of breast cancer stem cells and prolongs survival [55]. Successful immunotherapy of malignant tumours by using NK cells is summarized in [56].

The cytokine therapy targets predicted are IL-10 and IL-12 in figure 9*b*. Endogenous IL-10 inhibits inflammatory cytokine production and hampers the development of Treg cells and MDSCs, two key components of the immunosuppressive tumour microenvironment [57]. A potentially beneficial role of IL-12 is demonstrated in directly limiting the malignant phenotype of cancer stem cells [58].

We also predicted the effects of combination immunotherapy. This is according to the landscape barrier change which

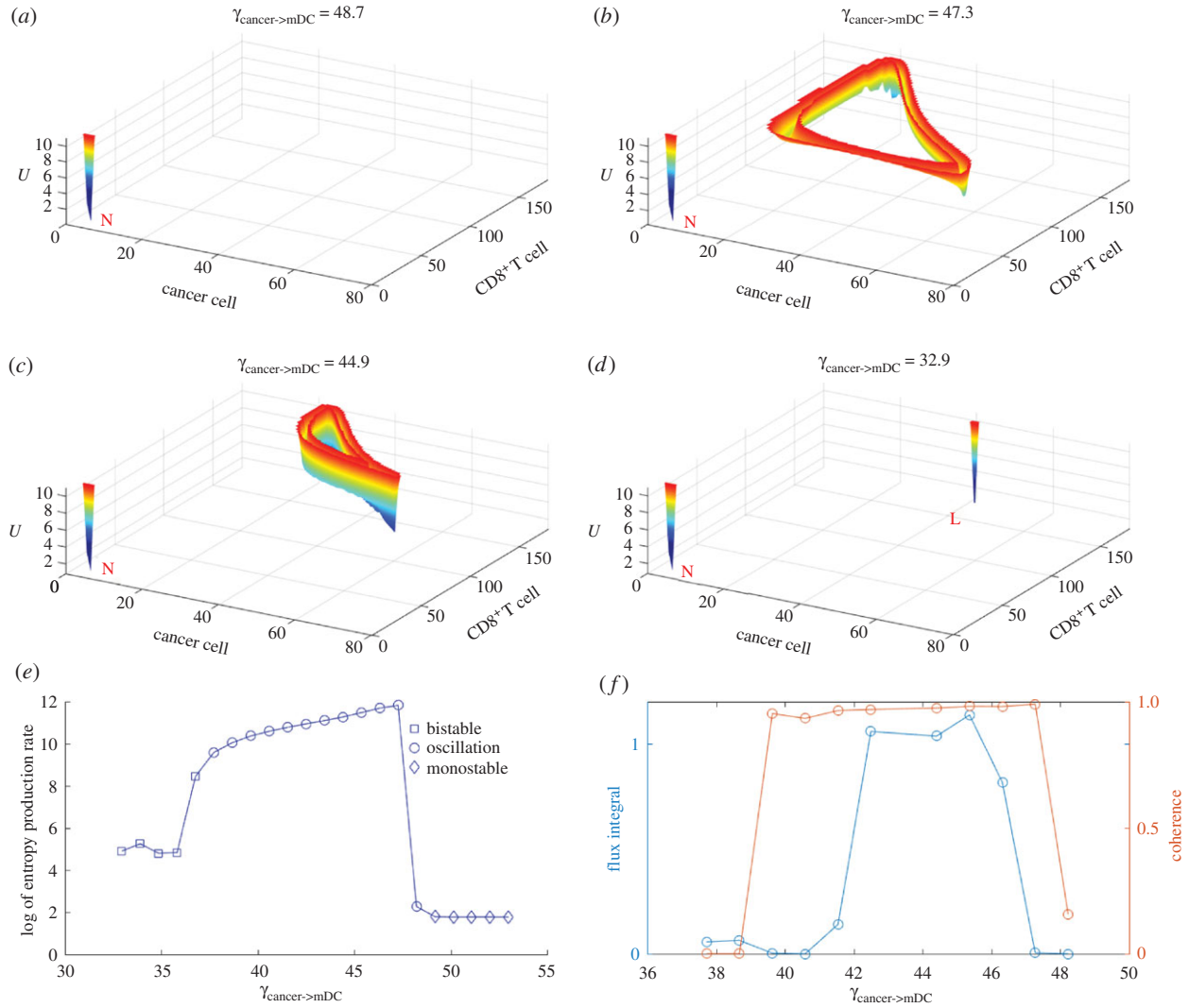

Figure 8. The landscape topography of the oscillation switch along with a decrease in $\gamma_{\text{cancer->mDC}}$. (*a*) Emergence of the normal state with $\gamma_{\text{cancer->mDC}} = 48.7$. (*b* and *c*) Coexistence of the normal state and the limit cycle with $\gamma_{\text{cancer->mDC}}$ from 47.3 to 44.9. (*d*) Emergence of the normal state and the low cancer state with $\gamma_{\text{cancer->mDC}} = 32.9$. (*e*) Entropy production rate of monostability, bistability and oscillation. (*f*) Flux integral and coherence of oscillation.

leads to higher stability/less stability of the cancer basin of attraction. The combination injection of every two types of cells or cytokines is predicted in figure 10. The values in the colour matrix represent the degrees of therapeutic effect. The red colour represents a positive therapeutic effect, while the blue colour represents a negative therapeutic effect. The two most effective combinations are NK cells with IL-10 and mDCs with IL-10.

3. Discussion

The relationship between cancer and immunity is complex and the underlying mechanism of the tumorigensis and development in the immune microenvironment is still unclear. In this study, a comprehensive cancer–immunity model is built including cancer cells, 12 types of immune cells and 13 types of cytokines. Their regulations are classified into three types of interactions: cell–cell interaction, cytokine–cell interaction and cell–cytokine production. There are three types of steady-state basins of attractors: normal state (N), low cancer state (L) and high cancer state (H). It is interesting that adaptive immunity of cancer is inhibited in the high cancer state compared with the low cancer state, although the innate immunity is normal. It has been reported that patients with a lower $CD8^+$ level have a higher T-stage of the tumour and a higher relapse rate [59].

We provide a physical view of cancer tumorigenesis and development. Cancer cells change the characteristics of the immune system by changing interaction strengths. Along the cancer progression under the immune system, six stages with different characteristics emerge in sequence (figure 6). Interestingly, they correspond to three phases: elimination, equilibrium and escape in the immunoediting framework [37]. This also suggests that the low cancer state is the source state and the high cancer state is the result of the evolution originating from cancer immune dynamics. The cancer cell concentration level in the high cancer state increases faster than that in the low cancer state with cancer development. The high cancer state moves to HH at stage 5, while the low cancer state moves to HH at stage 6. In other words, unlucky patients with a high cancer state at stage 3 or 4 will die earlier owing to the rapid cancer cell concentration increase under cancer development. The steady-state attractor originating from the high cancer state only exists within a specific cancer immunity, neither too low nor too high. This provides an opportunity for cancer to remain in

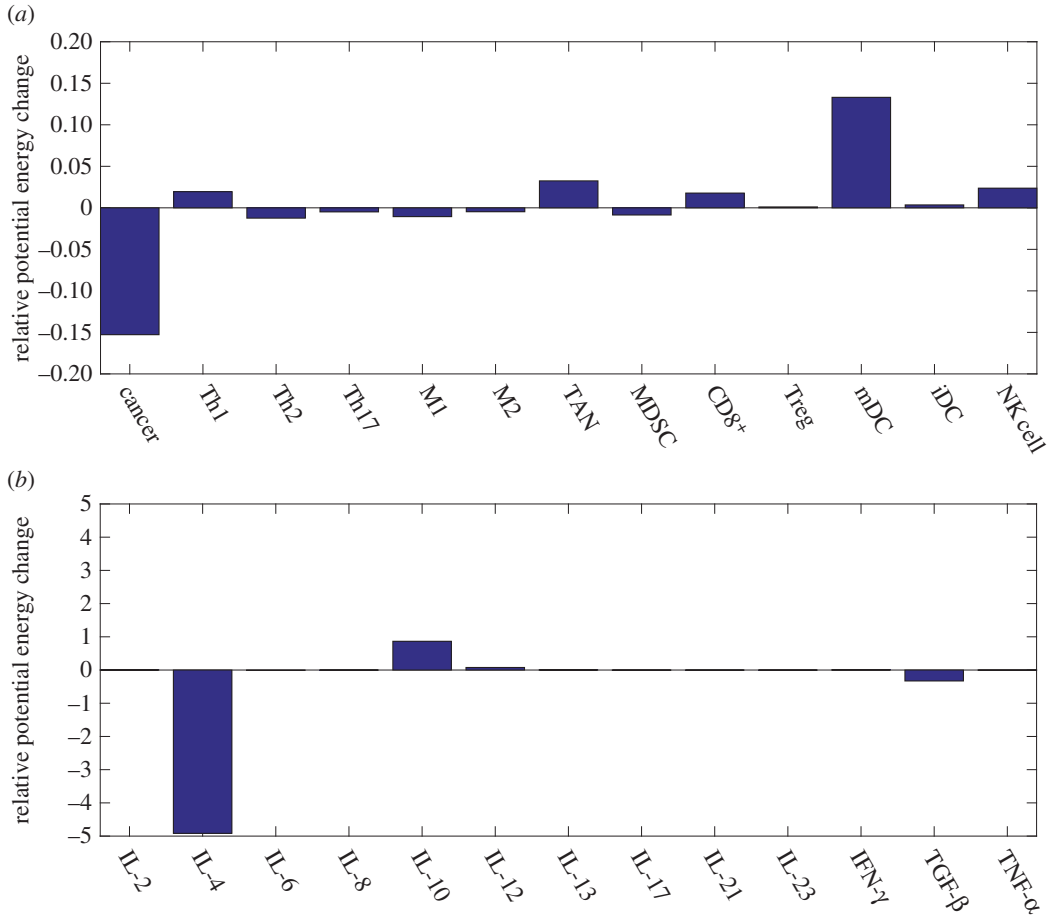

Figure 9. Predictions for immunotherapy targets based on barrier changes for cells and cytokine injections. (*a*) Relative potential energy changes of the cell injections. (*b*) Relative potential energy changes of the cytokine injections. The parameter $c_i = 0.2$.

a potentially malignant stage (high cancer state at stage 3 or 4). Thus, it is questioned whether it is possible that cancer displays different phenotypes even in the same genotype, condition, microenvironment or process due to the underlying mechanism of cancer immune dynamic interactions. Perhaps the immune system increases the variety and complexity of cancer.

Limit cycle oscillations emerge upon certain cell–cell interactions. It is common that oscillations occur in the immune system [60]. Periodic oscillations have been observed in cancer through analysing blood cell counts [61]. It is reasonable that the oscillatory phenomenon occurs in the cancer–immune system. Although it has been discussed whether the oscillation is encountered by the delay of the immune response with contradictory results [51,62–64], the biological functions or components leading to oscillation have not been studied. In our work, we find that the module with cancer cells, mDCs and $CD8^+$ leads to the oscillation of the cancer–immune system. These three types of cells play an important role in the cancer–immune system. Through analysis of the entropy production rate, flux integral and coherence, this suggest that tumorigenesis and cancer recovery processes may need to go through cancer–immune oscillation and consume more energy.

Three types of cells and two types of cytokines are predicted in our model, all of which have been reported as effective for curing cancer or produced as vaccines [55–58]. Combinations of therapy have been suggested to be more effective. We predicted two of the most effective combinations for immunotherapy. The mathematical model in this study is built based on prior knowledge of the interactions of the immune system. There are still many undiscovered interactions in the immune system. This limits the complete quantitative descriptions of the immune system from the mathematical models. Although the current cancer–immune model contains 12 types of immune cells and 13 types of cytokines, the complexity between the cancer and the immune system is still underestimated. In addition, some other issues such as gene expressions in different cells are not considered owing to their complexity. Therefore, a model with genetic expression, immune cells, cytokines and cancer microenvironment changes can hopefully be used for studying the cancer mechanism and cancer therapy.

4. Material and methods

4.1. Self-consistent mean field approximation

The evolution of the probability distribution on the dynamic system can be described by the probabilistic diffusion equations. Given the state $P(X_1, X_2, \ldots, X_n, t)$, where $X_1, X_2, \ldots, X_n$ represent the concentration of the cells or the cytokines, it is hard to exactly solve the high-dimensional partial differential equations. Here, we apply self-consistent mean field approximation of individual variables. The probability $P(X_1, X_2, \ldots, X_n, t)$ is split into the products of probability of the individual variable, $\prod P(X_i,t)$, according to [11,65–68]. Thus, the dimensionality of the system is reduced to $M \times N$ from M^N, which makes the computation and storage tractable.

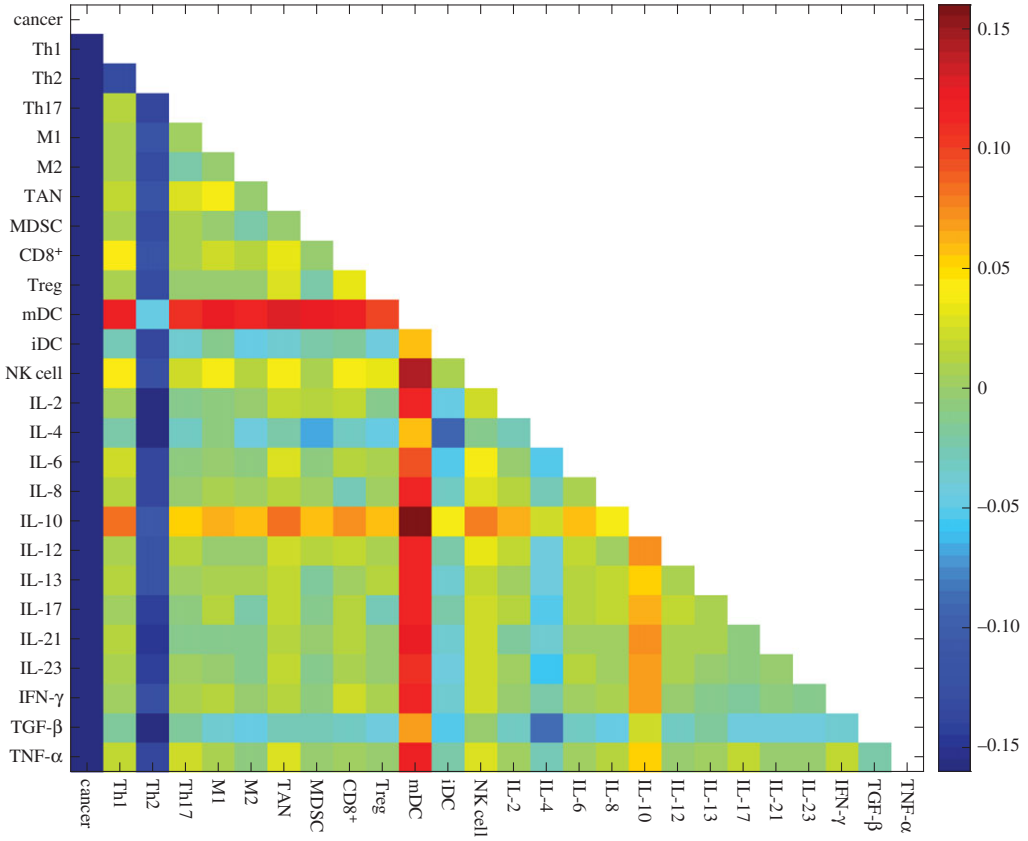

Figure 10. Predictions for combinations of immunotherapy based on barrier changes upon cell and cytokine injection. Red colour represents positive therapy and blue colour represents negative therapy. The parameter $c_i = 0.1$.

However, it is often difficult to solve the self-consistent mean field equation due to its nonlinearity. We start from the moment equations. In principle, once all moments are known, we can obtain the probability distributions of the dynamic system. Here, a Gaussian distribution ansatz is used to calculate the probability for approximation, and two moments, the mean and the variance, need to be known.

When the diffusion coefficient D is small, the moment equations can be approximated to [69]:

$$\dot{\bar{x}}(t) = F(\bar{x}(t)) \tag{4.1}$$

and

$$\dot{\sigma}(t) = \sigma(t)A^{\mathrm{T}}(t) + A(t)\sigma(t) + 2D(\bar{x}(t)). \tag{4.2}$$

Here, $\bar{x}(t)$ is the mean of a certain variable and $\sigma(t)$ is the covariance matrix of the dynamic system evolution. $A(t)$ is a tensor and its matrix element is $A_{ij} = \partial F_i(x(t))/\partial x_j(t)$. $A^{\mathrm{T}}(t)$ is the transpose of $A(t)$. In terms of these equations, we can solve $x(t)$ and $\sigma(t)$. The diagonal elements of $\sigma(t)$ are considered. Therefore, the evolution of the probabilistic distribution for each variable can be expressed by Gaussian approximation determined by the mean and variance,

$$P(x,t) = \frac{1}{\sqrt{2\pi\sigma(t)}} \mathrm{e}^{-(x-\bar{x}(t))^2/2\sigma(t)}. \tag{4.3}$$

The equation above is the expression of the probability for one steady state. For a multistable system, the total probability is equal to the probability of overlap for all the steady states. The multistable system probability of x has the form: $P(x,t) = \sum w_i P_i(x)$. Here the weight factor w_i can be obtained through Langevin simulation. Finally, the landscape can be quantified through the steady-state probability, $U(x) = -\ln P_{\mathrm{ss}}(x)$.

4.2. Langevin dynamics method

For a dynamic system in noisy fluctuating environments, the dynamics is often described by ODEs as $\dot{x} = F(x) + \zeta$. Here, $x(t)$ represents the vector of the cell concentration and the cytokine concentration. $F(x)$ is the vector for the driving force of these cell–cell interactions, cytokine–cell interactions or cell–cytokine production. External noise and intrinsic noise are of significance to biological systems [70]. So the noise term ζ is added to the force $\dot{x} = F(x)$, the average dynamics of the system. The noise term ζ is assumed to follow a Gaussian distribution and the mean correlations are given as: $\langle \zeta_j(x,t) \rangle = 0$ and $\langle \zeta_i(x,t)\zeta_j(x,t') \rangle = 2D_{ij}\delta_{ij}\delta(t-t')$ ($\delta_{ij} = 1$ for $i = j$ and $\delta_{ij} = 0$ for $i \neq j$). Here $\delta(t)$ is the Dirac delta function and D is the diffusion coefficient matrix. The noise term is associated with the intensity of cellular fluctuations either from the environmental external fluctuations or from the intrinsic fluctuations. Under long-time Langevin dynamics simulations, we can obtain the steady-state distribution $P(x)$ for the state variable x through statistics. Finally, the potential landscape is obtained by $U = -\ln(P(x))$.

Data accessibility. Codes and parameters can be found in doi:10.6084/m9.figshare.5053624.

Author's contributions. J.W. designed the research; W.L. and J.W. performed the research; W.L. and J.W. analysed the data; and W.L. and J.W. wrote the paper.

Competing interests. We declare we have no competing interests.

Funding. This study was supported by NSFC grant no. 91430217, and MOST China grant nos. 2016YFA0203200 and 2013YQ170585. J.W. is grateful for support from grant no. NSF-PHY-76066.

Acknowledgements. W.L. thanks K. Zhang, Dr L. Xu, Dr F. Zhang, L. Zhao and C. Yu for discussions and comments.

References

1. Gajewski TF, Schreiber H, Fu Y-X. 2013 Innate and adaptive immune cells in the tumor microenvironment. *Nat. Immunol.* **14**, 1014–1022. (doi:10.1038/ni.2703)
2. DuBois RN, Wang D. 2015 Immunosuppression associated with chronic inflammation in the tumor microenvironment. *Carcinogenesis* **36**, 1085–1093. (doi:10.1093/carcin/bgv123)
3. Weinberg RA, Hanahan D. 2011 Hallmarks of cancer: the next generation. *Cell* **144**, 646–674. (doi:10.1016/j.cell.2011.02.013)
4. Sabado RL, Bhardwaj N. 2015 Cancer immunotherapy: dendritic-cell vaccines on the move. *Nature* **519**, 300–301. (doi:10.1038/nature14211)
5. Eftimie R, Bramson JL, Earn DJD. 2011 Interactions between the immune system and cancer: a brief review of non-spatial mathematical models. *Bull. Math. Biol.* **73**, 2–32. (doi:10.1007/s11538-010-9526-3)
6. Wilkie KP, Hahnfeldt P. 2013 Mathematical models of immune-induced cancer dormancy and the emergence of immune evasion. *Interface Focus* **3**, 20130010. (doi:10.1098/rsfs.2013.0010)
7. Pappalardo F, Pennisi M, Ricupito A, Topputo F, Bellone M. 2014 Induction of t-cell memory by a dendritic cell vaccine: a computational model. *Bioinformatics* **30**, 1884–1891. (doi:10.1093/bioinformatics/btu059)
8. Wang J, Xu L, Wang E. 2008 Potential landscape and flux framework of nonequilibrium networks: robustness, dissipation, and coherence of biochemical oscillations. *Proc. Natl Acad. Sci. USA* **105**, 12 271–12 276. (doi:10.1073/pnas.0800579105)
9. Wang J, Zhang K, Xu L, Wang E. 2011 Quantifying the Waddington landscape and biological paths for development and differentiation. *Proc. Natl Acad. Sci. USA* **108**, 8257–8262. (doi:10.1073/pnas.1017017108)
10. Wang J. 2015 Landscape and flux theory of non-equilibrium dynamical systems with application to biology. *Adv. Phys.* **64**, 1–137. (doi:10.1080/00018732.2015.1037068)
11. Li C, Wang J. 2013 Quantifying cell fate decisions for differentiation and reprogramming of a human stem cell network: landscape and biological paths. *PLoS Comput. Biol.* **9**, e1003165. (doi:10.1371/journal.pcbi.1003165)
12. Li C, Wang J. 2013 Quantifying Waddington landscapes and paths of non-adiabatic cell fate decisions for differentiation, reprogramming and transdifferentiation. *J. R. Soc. Interface* **10**, 20130787. (doi:10.1098/rsif.2013.0787)
13. Li C, Wang J. 2014 Quantifying the underlying landscape and paths of cancer. *J. R. Soc. Interface* **11**, 20140774. (doi:10.1098/rsif.2014.0774)
14. Li C, Wang J. 2015 Quantifying the landscape for development and cancer from a core cancer stem cell circuit. *Cancer. Res.* **75**, 2607–2618. (doi:10.1158/0008-5472.CAN-15-0079)
15. Yan H, Zhao L, Hu L, Wang X, Wang E, Wang J. 2013 Nonequilibrium landscape theory of neural networks. *Proc. Natl Acad. Sci. USA* **110**, E4185–E4194. (doi:10.1073/pnas.1310692110)
16. Yan H, Zhang K, Wang J. 2016 Physical mechanism of mind changes and tradeoffs among speed, accuracy, and energy cost in brain decision making: landscape, flux, and path perspectives. *Chin. Phys. B* **25**, 078702. (doi:10.1088/1674-1056/25/7/078702)
17. Li C, Wang E, Wang J. 2012 Landscape topography determines global stability and robustness of a metabolic network. *ACS Synth. Biol.* **1**, 229–239. (doi:10.1021/sb300020f)
18. Lapidus S, Han B, Wang J. 2008 Intrinsic noise, dissipation cost, and robustness of cellular networks: the underlying energy landscape of MAPK signal transduction. *Proc. Natl Acad. Sci. USA* **105**, 6039–6044. (doi:10.1073/pnas.0708708105)
19. Zhang F, Xu L, Zhang K, Wang E, Wang J. 2012 The potential and flux landscape theory of evolution. *J. Chem. Phys.* **137**, 065102. (doi:10.1063/1.4734305)
20. Xu L, Zhang F, Zhang K, Wang E, Wang J. 2014 The potential and flux landscape theory of ecology. *PLoS ONE* **9**, e86746. (doi:10.1371/journal.pone.0086746)
21. Wilke CM, Kryczek I, Wei S, Zhao E, Wu K, Wang G, Zou W. 2011 Th17 cells in cancer: help or hindrance? *Carcinogenesis* **32**, 643–649. (doi:10.1093/carcin/bgr019)
22. Strioga M, Schijns V, Powell DJ, Pasukoniene V, Dobrovolskiene N, Michalek J. 2012 Dendritic cells and their role in tumor immunosurveillance. *Innate Immun.* **19**, 98–111. (doi:10.1177/1753425912449549)
23. Galdiero MR, Garlanda C, Jaillon S, Marone G, Mantovani A. 2013 Tumor associated macrophages and neutrophils in tumor progression. *J. Cell. Physiol.* **228**, 1404–1412. (doi:10.1002/jcp.24260)
24. Hemdan NYA. 2013 Anti-cancer versus cancer-promoting effects of the interleukin-17-producing t helper cells. *Immunol. Lett.* **149**, 123–133. (doi:10.1016/j.imlet.2012.11.002)
25. Qi W, Huang X, Wang J. 2013 Correlation between th17 cells and tumor microenvironment. *Cell. Immunol.* **285**, 18–22. (doi:10.1016/j.cellimm.2013.06.001)
26. Ma Y, Shurin GV, Peiyuan Z, Shurin MR. 2013 Dendritic cells in the cancer microenvironment. *J. Cancer* **4**, 36–44. (doi:10.7150/jca.5046)
27. Dudek AM, Martin S, Garg AD, Agostinis P. 2013 Immature, semi-mature, and fully mature dendritic cells: toward a DC-cancer cells interface that augments anticancer immunity. *Front. Immunol.* **4** (doi:10.3389/fimmu.2013.00438)
28. Khaled YS, Ammori BJ, Elkord E. 2013 Myeloid-derived suppressor cells in cancer: recent progress and prospects. *Immunol. Cell Biol.* **91**, 493–502. (doi:10.1038/icb.2013.29)
29. Jiang J, Guo W, Liang X. 2014 Phenotypes, accumulation, and functions of myeloid-derived suppressor cells and associated treatment strategies in cancer patients. *Hum. Immunol.* **75**, 1128–1137. (doi:10.1016/j.humimm.2014.09.025)
30. Lewis CE. 2006 Distinct role of macrophages in different tumor microenvironments. *Cancer Res.* **66**, 605–612. (doi:10.1158/0008-5472.CAN-05-4005)
31. Wolf D, Sopper S, Pircher A, Gastl G, Wolf AM. 2015 Treg(s) in cancer: friends or foe? *J. Cell. Physiol.* **230**, 2598–2605. (doi:10.1002/jcp.25016)
32. Tran Janco JM, Lamichhane P, Karyampudi L, Knutson KL. 2015 Tumor-infiltrating dendritic cells in cancer pathogenesis. *J. Immunol.* **194**, 2985–2991. (doi:10.4049/jimmunol.1403134)
33. Powell DR, Huttenlocher A. 2016 Neutrophils in the tumor microenvironment. *Trends Immunol.* **37**, 41–52. (doi:10.1016/j.it.2015.11.008)
34. Wörmann SM, Diakopoulos KN, Lesina M, Algül H. 2013 The immune network in pancreatic cancer development and progression. *Oncogene* **33**, 2956–2967. (doi:10.1038/onc.2013.257)
35. Morvan MG, Lanier LL. 2015 NK cells and cancer: you can teach innate cells new tricks. *Nat. Rev. Cancer* **16**, 7–19. (doi:10.1038/nrc.2015.5)
36. Sokol CL, Barton GM, Farr AG, Medzhitov R. 2007 A mechanism for the initiation of allergen-induced T helper type 2 responses. *Nat. Immunol.* **9**, 310–318. (doi:10.1038/ni1558)
37. Dunn GP, Bruce AT, Ikeda H, Old LJ, Schreiber RD. 2002 Cancer immunoediting: from immunosurveillance to tumor escape. *Nat. Immunol.* **3**, 991–998. (doi:10.1038/ni1102-991)
38. Garrido F, Aptsiauri N, Doorduijn EM, Lora AMG, van Hall T. 2016 The urgent need to recover MHC class I in cancers for effective immunotherapy. *Curr. Opin. Immunol.* **39**, 44–51. (doi:10.1016/j.coi.2015.12.007)
39. de Pillis LG, Gu W, Radunskaya AE. 2006 Mixed immunotherapy and chemotherapy of tumors: modeling, applications and biological interpretations. *J. Theor. Biol.* **238**, 841–862. (doi:10.1016/j.jtbi.2005.06.037)
40. Kirschner D, Panetta JC. 1998 Modeling immunotherapy of the tumor–immune interaction. *J. Math. Biol.* **37**, 235–252. (doi:10.1007/s002850050127)
41. Lu M, Huang B, Hanash SM, Onuchic JN, Ben-Jacob E. 2014 Modeling putative therapeutic implications of exosome exchange between tumor and immune cells. *Proc. Natl Acad. Sci. USA* **111**, E4165–E4174. (doi:10.1073/pnas.1416745111)
42. Gabrilovich DI, Nagaraj S. 2009 Myeloid-derived suppressor cells as regulators of the immune system. *Nat. Rev. Immunol.* **9**, 162–174. (doi:10.1038/nri2506)

43. DeNardo DG, Coussens LM. 2007 Inflammation and breast cancer. Balancing immune response: crosstalk between adaptive and innate immune cells during breast cancer progression. *Breast Cancer Res.* **9**, 212. (doi:10.1186/bcr1746)
44. Kusmartsev S, Gabrilovich D. 2002 Immature myeloid cells and cancer-associated immune suppression. *Cancer Immunol. Immunother.* **51**, 293–298. (doi:10.1007/s00262-002-0280-8)
45. Vicari AP, Caux C, Trinchieri G. 2002 Tumour escape from immune surveillance through dendritic cell inactivation. *Semin. Cancer Biol.* **12**, 33–42. (doi:10.1006/scbi.2001.0400)
46. Ferrantini M, Capone I, Belardelli F. 2008 Dendritic cells and cytokines in immune rejection of cancer. *Cytok. Growth Factor Rev.* **19**, 93–107. (doi:10.1016/j.cytogfr.2007.10.003)
47. Titu LV, Monson JR, Greenman J. 2002 The role of $CD8^+$ T cells in immune responses to colorectal cancer. *Cancer Immunol. Immunother.* **51**, 235–247. (doi:10.1007/s00262-002-0276-4)
48. Marcus A, Gowen BG, Thompson TW, Iannello A, Ardolino M, Deng W, Wang L, Shifrin N, Raulet DH. 2014 Recognition of tumors by the innate immune system and natural killer cells. *Adv. Immunol.* **122**, 91–128. (doi:10.1016/B978-0-12-800267-4.00003-1)
49. Wertel I. 2008 The role of dendritic cells in cytotoxic immune response regulation in ovarian cancer microenvironment. *Front. Biosci.* **13**, 2177. (doi:10.2741/2833)
50. Lejeune O, Chaplain MAJ, ElAkili I. 2008 Oscillations and bistability in the dynamics of cytotoxic reactions mediated by the response of immune cells to solid tumours. *Math. Comput. Model.* **47**, 649–662. (doi:10.1016/j.mcm.2007.02.026)
51. Bi P, Ruan S, Zhang X. 2014 Periodic and chaotic oscillations in a tumor and immune system interaction model with three delays. *Chaos* **24**, 023101. (doi:10.1063/1.4870363)
52. Banchereau J, Steinman RM. 1998 Dendritic cells and the control of immunity. *Nature* **392**, 245–252. (doi:10.1038/32588)
53. Evans CM, Findley GL. 1999 A new transformation for the Lotka–Volterra problem. *J. Math. Chem.* **25**, 105–110. (doi:10.1023/A:1019172114300)
54. Koch M. 2016 Cancer immunotherapy booster. *Cell* **165**, 253–255. (doi:10.1016/j.cell.2016.04.055)
55. Pham PV *et al*. 2016 Targeting breast cancer stem cells by dendritic cell vaccination in humanized mice with breast tumor: preliminary results. *OncoTargets Ther.* **9**, 4441–4451. (doi:10.2147/OTT.S105239)
56. Cheng M, Chen Y, Xiao W, Sun R, Tian Z. 2013 NK cell-based immunotherapy for malignant diseases. *Cell. Mol. Immunol.* **10**, 230–252. (doi:10.1038/cmi.2013.10)
57. Tanikawa T, Wilke CM, Kryczek I, Chen GY, Kao J, Nunez G, Zou W. 2011 Interleukin-10 ablation promotes tumor development, growth, and metastasis. *Cancer Res.* **72**, 420–429. (doi:10.1158/0008-5472.CAN-10-4627)
58. Yin XL, Wang N, Wei X, Xie GF, Li JJ, Liang HJ. 2012 Interleukin-12 inhibits the survival of human colon cancer stem cells in vitro and their tumor initiating capacity in mice. *Cancer Lett.* **322**, 92–97. (doi:10.1016/j.canlet.2012.02.015)
59. Mlecnik B *et al.* 2011 Histopathologic-based prognostic factors of colorectal cancers are associated with the state of the local immune reaction. *J. Clin. Oncol.* **29**, 610–618. (doi:10.1200/JCO.2010.30.5425)
60. Stark J, Chan C, George AJT. 2007 Oscillations in the immune system. *Immunol. Rev.* **216**, 213–231. (doi:10.1111/j.1600-065X.2007.00501.x)
61. Fortin P, Mackey MC. 1999 Periodic chronic myelogenous leukaemia: spectral analysis of blood cell counts and aetiological implications. *Br. J. Haematol.* **104**, 336–345. (doi:10.1046/j.1365-2141.1999.01168.x)
62. d'Onofrio A, Gatti F, Cerrai P, Freschi L. 2010 Delay-induced oscillatory dynamics of tumour–immune system interaction. *Math. Comput. Model.* **51**, 572–591. (doi:10.1016/j.mcm.2009.11.005)
63. Feyissa S, Banerjee S. 2013 Delay-induced oscillatory dynamics in humoral mediated immune response with two time delays. *Nonlinear Anal. Real World Appl.* **14**, 35–52. (doi:10.1016/j.nonrwa.2012.05.001)
64. Bodnar M, Foryś U. 2016 Delays do not cause oscillations in a corrected model of humoral mediated immune response. *Appl. Math. Comput.* **289**, 7–21. (doi:10.1016/j.amc.2016.05.006)
65. Li C, Wang J. 2014 Landscape and flux reveal a new global view and physical quantification of mammalian cell cycle. *Proc. Natl Acad. Sci. USA* **111**, 14 130–14 135. (doi:10.1073/pnas.1408628111)
66. Wang J, Li C, Wang E. 2010 Potential and flux landscapes quantify the stability and robustness of budding yeast cell cycle network. *Proc. Natl Acad. Sci. USA* **107**, 8195–8200. (doi:10.1073/pnas.0910331107)
67. Sasai M, Wolynes PG. 2003 Stochastic gene expression as a many-body problem. *Proc. Natl Acad. Sci. USA* **100**, 2374–2379. (doi:10.1073/pnas.2627987100)
68. Zhang B, Wolynes PG. 2014 Stem cell differentiation as a many-body problem. *Proc. Natl Acad. Sci. USA* **111**, 10 185–10 190. (doi:10.1073/pnas.1408561111)
69. Van Kampen NG. 1992 *Stochastic processes in chemistry and physics*. Amsterdam, The Netherlands: North Holland.
70. Kærn M, Elston TC, Blake WJ, Collins JJ. 2005 Stochasticity in gene expression: from theories to phenotypes. *Nat. Rev. Genet.* **6**, 451–464. (doi:10.1038/nrg1615)